

# RSC Advances



This is an *Accepted Manuscript*, which has been through the Royal Society of Chemistry peer review process and has been accepted for publication.

*Accepted Manuscripts* are published online shortly after acceptance, before technical editing, formatting and proof reading. Using this free service, authors can make their results available to the community, in citable form, before we publish the edited article. This *Accepted Manuscript* will be replaced by the edited, formatted and paginated article as soon as this is available.

You can find more information about *Accepted Manuscripts* in the [Information for Authors](#).

Please note that technical editing may introduce minor changes to the text and/or graphics, which may alter content. The journal's standard [Terms & Conditions](#) and the [Ethical guidelines](#) still apply. In no event shall the Royal Society of Chemistry be held responsible for any errors or omissions in this *Accepted Manuscript* or any consequences arising from the use of any information it contains.

Cite this: DOI: 10.1039/c0xx00000x

www.rsc.org/xxxxxx

ARTICLE TYPE

# Simple one-pot synthesis of ZnO/Ag heterostructures and the application in visible-light-responsive photocatalysis

Yuming Dong, \* Cuiyun Feng, Pingping Jiang, Guangli Wang, Kun Li, Hongyan Miao

Received (in XXX, XXX) Xth XXXXXXXXX 20XX, Accepted Xth XXXXXXXXX 20XX

DOI: 10.1039/b000000x

The development of efficient visible-light-driven photocatalysts remains one of the greatest scientific challenges of this century. In this paper, visible light active ZnO/Ag heterostructures have been synthesized in a large-scale by a simple one-pot synthesis method. Influence of Zn/Ag ratio on the properties of heterostructures was investigated in detail. In light of the formation process of heterostructures, ZnO rods and Ag nanoparticles can link each other by strong bond due to the bridging effect of NH<sub>3</sub>, which is found to be essential for the efficient visible-light-responsive activity and stability. These heterostructures were characterized by transmission electron microscopy (TEM), energy-dispersive X-ray spectroscopy (EDX), X-ray diffraction (XRD), X-ray fluorescence, Raman and UV-vis spectroscopy. These results indicate that ZnO/Ag composition is well-constructed with a band gap of 2.85 eV. Moreover, photocatalytic experiments show that these ZnO/Ag heterostructures are robust and exhibit high photocatalytic activity for the efficient separation of electron-hole pairs and the subsequent generation of hydroxyl radicals.

## 1. Introduction

One of the great challenges in the research of photocatalysts is to rationally design materials for harvesting solar energy. In this regard, nanostructures have attracted significant interest because their optical and electrical properties can be tuned by adjusting the size and morphology. One of the methods to increase the efficiency of the photocatalytic activity is to develop heterogeneous metal/semiconductor nanocomposite materials.<sup>1-6</sup> ZnO is a widely used semiconductor with a band gap about 3.37 eV and an exciton binding energy of 60 meV.<sup>7</sup> For its low cost and environmental friendliness, ZnO is regarded as a promising photocatalyst.<sup>8</sup> Metal particle of Au or Ag with an intense localized surface plasmon resonance (LSPR) peak can act as a nano-antenna for light trapping, resulting from photoexcitation of the LSPR peak to form a locally enhanced electric field in the proximity of metal nanoparticles.<sup>9-10</sup> Recently, novel hybridized structures of silver and ZnO were designed and studied as efficient photocatalysts. These ZnO/Ag heterostructure revealed better photoelectric performance and photocatalytic properties than pure ZnO.<sup>11,12</sup> In spite of these great achievements, there are two main limitations: most of ZnO/Ag composites suffer from the narrow absorption spectral range and could be excited by UV light only. Because about half of the solar energy is at the visible region, this is a great drawback for practical application. Even though, the visible light driven photocatalysts based on ZnO/Ag have been reported and revealed desirable performance, these visible light active ZnO/Ag nanocomposites were prepared through complicated procedures with special instruments, such as ITO glass, liquid arc discharge or laser instrument.<sup>13</sup> Thus, the synthesis of visible-light-responsive ZnO/Ag heterostructure by a

simple method becomes another main challenge and this requires a novel preparation strategy.

Herein, we report an economical and large-scale one-pot synthesis route of the ZnO/Ag heterostructure as visible-light-responsive photocatalyst. In this study, ammonia and Zn powder were added to the solution of NaOH containing AgNO<sub>3</sub>. After heating in air, the ZnO/Ag compositions were obtained. Using NH<sub>3</sub> as a good bridging ligand leads to strong bonding between Ag nanoparticles and ZnO rods and a band gap of 2.85 eV was obtained, which is essential for the robust visible light photocatalytic activity and stability.

## 2. Experimental

### 2.1 Materials

Zinc powder (Zn), sodium hydroxide (NaOH), silver nitrate (AgNO<sub>3</sub>), 2wt% aqueous ammonium solution (NH<sub>3</sub>·H<sub>2</sub>O), terephthalic acid (7.5×10<sup>-4</sup> mol/L) and xylene orange (2 g/L) were all analytical grade and used without further purification. Deionized water was employed throughout experiments.

### 2.2 Preparation of ZnO/Ag heterostructures with different Zn/Ag ratio

ZnO/Ag heterostructures with different Zn/Ag ratio were synthesized through a simple one-pot synthesis method as follows. 100 mL of (2%) NH<sub>3</sub>·H<sub>2</sub>O was added to a solution of 30 mL NaOH (pH=11) containing various amounts of AgNO<sub>3</sub> (0.005 mol, 0.010 mol, 0.015 mol, 0.020 mol) in order to obtain the ZnO/Ag heterostructures with different Zn/Ag molar fraction (4:1, 4:2, 4:3, 4:4). After stirring for 1 h, 0.020 mol of Zn was

added into the previous solution, respectively. The resulting solution was stirred at room temperature for 2 h and then heated in the air at 160 °C for 16 h. The products were washed with water, and dried in the air at 100 °C for 12 h. For comparison, ZnO nanocrystals were also prepared according to the same preparation procedure of ZnO/Ag heterostructures without addition of AgNO<sub>3</sub>. The obtained ZnO/Ag heterostructure with Zn/Ag ratio of 4:4 was named as sample 1.

### 2.3 Control experiments for preparation of ZnO/Ag sample 1

To confirm the formation process of the ZnO/Ag heterostructure sample 1, control experiments to investigate the influence of Zn(NH<sub>3</sub>)<sub>4</sub><sup>2+</sup> and temperature were carried out as follows, and the products were named as sample 2 and sample 3 respectively. (1) Sample 2: Firstly, NH<sub>3</sub>·H<sub>2</sub>O, NaOH, AgNO<sub>3</sub> and Zn were mixed according to the same procedure and condition used in the preparations of sample 1. The resulting solution was stirred at room temperature for 2 h and then washed with water to remove the Zn(NH<sub>3</sub>)<sub>4</sub><sup>2+</sup>, and finally heated in the air at 160 °C for 16 h. (2) Sample 3: Firstly, NH<sub>3</sub>·H<sub>2</sub>O, NaOH, AgNO<sub>3</sub> and Zn were mixed according to the same procedure and condition used in the preparations of sample 1. Then the resulting solution was stirred at room temperature for 2 h and then heated in the air at 100 °C (lower than 160 °C for sample 1) for 16 h. The product was washed with water, and dried in the air at 100 °C for 12 h.

### 2.4 Characterization methods of catalyst

A D8 X-ray diffractometer (XRD, Bruker AXS, German) was employed using Cu K $\alpha$  radiation ( $\lambda = 0.15418$  nm) with a scanning rate of 4 °/min to verify the structures of the samples. X-ray fluorescence spectrometry (XRF) was carried out on an X-ray fluorescence spectrometer (ARL, Switzerland) to determine the ratio of ZnO and Ag. JEOL JEM-2010 transmission electron microscope (TEM) was used to examine the morphologies. Energy-dispersive X-ray spectroscopy (EDX) was taken on the TEM. In situ Raman spectra were taken on a confocal microscopic Raman spectrometer (Renishaw In-Via) with a 785 nm laser light irradiation. UV-vis diffuse reflectance spectra were measured on a Shimadzu UV-3600 spectrophotometer. Photoelectrochemical experiments were performed on a CHI 800C electrochemical workstation (Shanghai, China) with visible-light irradiation (>420nm) from a Xenon lamp (300W), and these experiments were done using a three-electrode cell configuration with a catalyst modified conductive glass as the working electrode, a platinum wire as the auxiliary electrode and a saturated Ag/AgCl electrode as the reference electrode.

### 2.5 Photocatalytic experiments

Xylenol orange (XO) was used as a representative dye indicator to evaluate the visible-light catalytic activity of ZnO/Ag heterostructure. 0.600 g of sample 1 photocatalyst was dispersed in a XO aqueous solution (26.7 mg/L, 150 mL). Before irradiation, the suspension was magnetically stirred for 1 h in the dark in order to reach adsorption-desorption equilibrium between the catalyst and the simulating pollutant. The mixture was then loaded to a reactor and continuously stirred during the exposure under visible-light irradiation (>420 nm) from a Xenon lamp (300 W). 3 mL aliquots were sampled and centrifuged to remove the catalyst at given time intervals. UV-vis spectrophotometer (TU-

1901, Beijing Pgeneral Instrument Co. Ltd.) was used to determinate the concentrations of the target pollutants (XO) at 574 nm. For comparison, the catalytic activities of ZnO/Ag heterostructures with different Zn/Ag ratio (4:1, 4:2, 4:3), sample 2, sample 3 and pure ZnO were also evaluated in the same way.

### 2.6 Determination of active oxidative species

Terephthalic acid was used as a fluorescence probe for hydroxyl radicals. The ZnO/Ag heterostructures photocatalyst were illuminated in the presence of terephthalic acid with same light source. The fluorescence intensity was measured using a fluorescence spectrophotometer (Cary Eclipse, US Varian Co. Ltd) and the fluorescence emission spectrum (excitation at 315 nm) of the solution was measured every 5 min during irradiation. To further confirm the main reactive specie responsible for the degradation of organic contaminants, the influence of tert-Butanol (a hydroxyl radical scavenger) on degradation of XO was investigated and 2 mol/L of tert-Butanol was used in the photocatalysis system.

## 3. Results and discussion

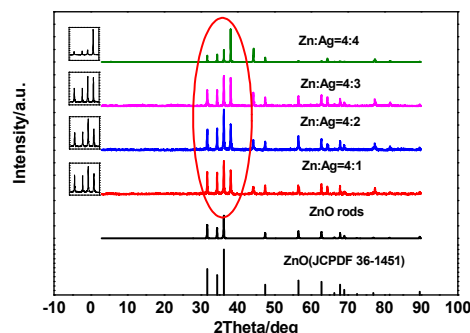


Fig. 1 XRD patterns of ZnO and ZnO/Ag heterostructures with different Zn/Ag ratio.

### 3.1 Influence of Zn/Ag ratio on ZnO/Ag heterostructures

ZnO/Ag heterostructures with different Zn/Ag ratio were prepared to investigate the influence of the amount of silver. Fig. 1 shows the XRD patterns of these samples. The lattice parameters of ZnO and the ZnO/Ag heterostructure with different loading amount of Ag were calculated by the software JADE 5.0 and listed in Table 1. The unit cell volume and lattice parameter expanded, and such extension could be ascribed to larger Ag cell volume ( $V = 68.23 \text{ \AA}^3$ ) compared to ZnO ( $47.62 \text{ \AA}^3$ ). Fig. 1 also shows the amplified XRD patterns in the 30–40° region, where a Bragg peak at 38.14° appears adjacent to the (1 0 0) diffraction of ZnO in presence of Ag. This peak can be indexed to the most prominent Bragg peak (1 1 1) for face-centered cubic (fcc) silver (JCPDF 04-0783), whose intensity increased with the decrease of Zn/Ag ratio (Fig. 1). This reveals the incorporated Ag grows orientationally along the rods of ZnO. The crystallite sizes of ZnO/Ag heterostructure also significantly increased as the increase in Ag loading (Table 1). It can be seen that the calculated crystallite sizes of ZnO/Ag heterostructure are much larger than that of pure ZnO. The slight variations in lattice parameters and crystallite sizes suggest Ag was well dispersed.

Table 1 the summarized characterization results

Sample	Crystal parameter				Degradation rate/%	K/min <sup>-1</sup>	Band gap energy/eV
	a/nm	c/nm	c/a	V/nm <sup>-3</sup>			
ZnO	3.24979	5.20658	1.602128	47.62	17.84	0.00658	3.15
Zn:Ag=4:1	3.25062	5.20713	1.601888	47.65	25.11	0.00978	3.14
Zn:Ag=4:2	3.25107	5.20964	1.602439	47.69	31.46	0.01195	3.13
Zn:Ag=4:3	3.25128	5.21283	1.603316	47.72	49.17	0.02201	3.13
Zn:Ag=4:4	3.25191	5.21783	1.604543	47.76	91.46	0.07165	2.85

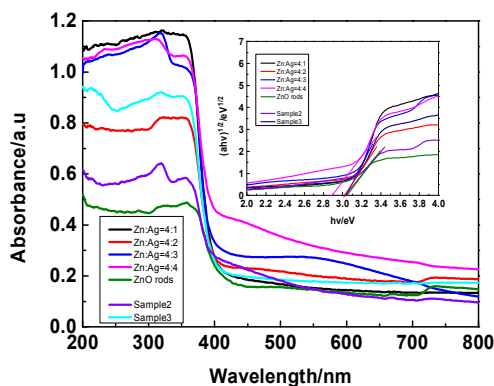


**Fig. 2** UV-visible diffuse reflectance spectra of ZnO/Ag heterostructures with different Zn/Ag ratio and the determination of the value of the band gap.

From the UV-vis diffuse reflectance spectrum (Fig. 2), with the increase of the amount of Ag, there is a obvious enhanced trend of the absorbance intensity in visible light range of 400-800 nm due to the surface plasmon resonance effect of Ag.<sup>9, 14</sup> For a semiconductor, the optical absorption near the band edge follows the equation  $ahv = A(hv - E_g)^{n/2}$ , in which  $a$ ,  $v$ ,  $A$ ,  $n$  and  $E_g$  are absorption coefficient, light frequency, proportionality constant, an integer ( $n = 1, 2, 4$  and  $6$ ) and band gap energy, respectively. According to this equation, the band gap values of ZnO/Ag heterostructures with different Zn/Ag ratio were calculated and listed in Table 1. From pure ZnO to ZnO/Ag heterostructures with Zn/Ag ratio of 4:1, 4:2 and 4:3, the band gap energy changed gradually from 3.15 eV to 3.13 eV. When the Zn/Ag ratio turned to 4:4, the band gap of the heterostructure was adjusted to 2.85 eV, which is significantly lower than that of the pure ZnO. This result clearly shows that absorption spectrum of ZnO was adjusted by formation of the visible light active ZnO/Ag heterostructures.

XO, a chemically stable dye molecule with a characteristic absorption peak at 574 nm, was chosen as a probe molecule to assess photocatalytic reactivity of these samples with different Zn/Ag ratio. As shown in Fig. 3A, the concentration of XO remains unchanged after 30 min of visible-light irradiation in the absence of catalyst. Compared with blank experiment, pure ZnO revealed weak catalytic activity. In presence of ZnO/Ag heterostructures, the degradation rate of XO was accelerated under the same reaction conditions. Among these heterostructures, the sample with Zn/Ag of 4:4 exhibited the

highest photocatalytic activity, which was nearly 91% XO removal within 30 min irradiation, while that was only 25% XO removal for sample of Zn/Ag=4:1. The apparent activity sequence of the catalysts are related to the Ag loading, according to the order as follows: Zn:Ag (4:4) > Zn:Ag (4:3) > Zn:Ag (4:2) > Zn:Ag(4:1) > Zn:Ag (4:0). The XO photodegradation on each ZnO/Ag heterostructure follows the pseudo-first-order kinetics model,  $\ln(C/C_0) = -kt$ , where  $C$  and  $C_0$  are the concentration of the dye in solution at time  $t$  and 0, respectively, and  $k$  is the pseudo-first-order rate constant.<sup>16</sup> The rate constant,  $k$  of XO photodegradation were derived from the  $-\ln(C/C_0) \sim t$  plots (Fig. 3B) and listed in Table 1. The rate constant changed from 0.00978 to 0.01195, 0.02201 and 0.07165 min<sup>-1</sup> with the Zn/Ag ratio increased from 4:1 to 4:2, 4:3 and 4:4. Considering the relationship of Zn/Ag ratio and optical properties of these ZnO/Ag heterostructures, the sample with Zn/Ag of 4:4 reveals better catalytic activity because more Ag was deposited on ZnO, leading to higher absorbance of visible light. Thus, the obtained ZnO/Ag heterostructure with Zn/Ag ratio of 4:4 was named as sample 1 and investigated further for the structure, formation process, photocatalytic application and mechanism.

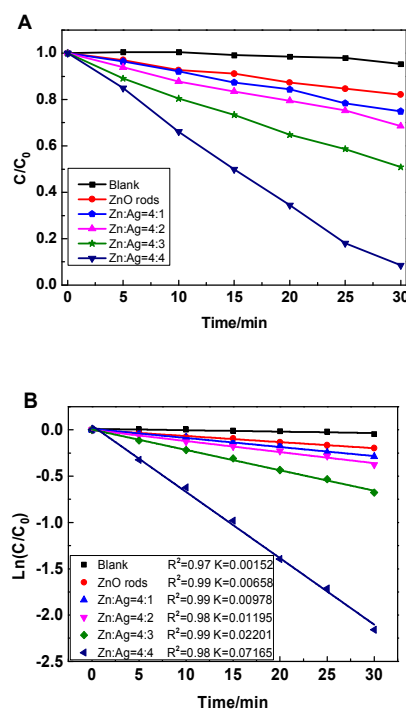


**Fig.3** (A) Photodegradation of XO over ZnO/Ag heterostructures with different Zn/Ag ratio samples; (B) plot of  $\ln(C/C_0)$  versus irradiation time under visible light ( $>420$  nm).

### 3.2 Structure and formation process of ZnO/Ag heterostructures

Taking sample 1 as an example, the structure of ZnO/Ag heterostructure was discussed further here.

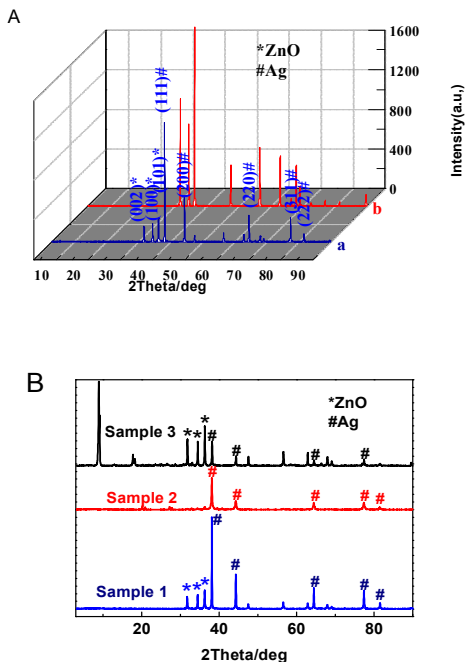


**Fig. 4** A: XRD patterns of ZnO/Ag heterostructure sample 1 (a) and pure ZnO (b); B: XRD patterns of sample 1, sample 2 and sample 3.

From the X-ray diffraction (XRD) patterns in Fig. 4A, pure ZnO sample can be indexed to a hexagonal wurtzite ZnO phase (JCPDF 36-1451). For the ZnO/Ag heterostructure sample 1, the peak at  $31.741^\circ$ ,  $34.400^\circ$  and  $36.319^\circ$  are the peaks of ZnO, and the peak at  $38.139^\circ$  is the peak of the face-centered cubic (fcc) silver (JCPDF 04-0783). Additionally, the peak at  $66.379^\circ$ ,  $76.940^\circ$  and  $81.382^\circ$  observed in pure ZnO sample disappeared in sample 1 due to the interaction of ZnO and Ag. From Fig. 5 (a), we can see the general morphology of the ZnO/Ag heterostructure, where the silver nanoparticles were loaded on the ZnO nanorods about 90-100 nm in diameter. Various Ag nanoparticles in the sizes ranging from 10 to 20 nm were affiliated well on the surface of ZnO nanorods. The red circle position in Fig. 5 (a) of single ZnO/Ag heterostructure was detected by Energy-dispersive X-ray (EDX) spectrum as shown in Fig. 5 (b). It was observed that this nanoparticle was composed of Ag, Zn and O, indicating it is mainly Ag nanoparticle. The average contents of these elements were obtained from the X-ray fluorescence spectrometry (XRF) with 58.63% of ZnO and 41.23% of Ag. The XRD, XRF and EDX results clearly show that sample 1 consists of ZnO and Ag. From EDX and TEM images, we propose that ZnO/Ag composition is well-constructed with ZnO rods and Ag particles.

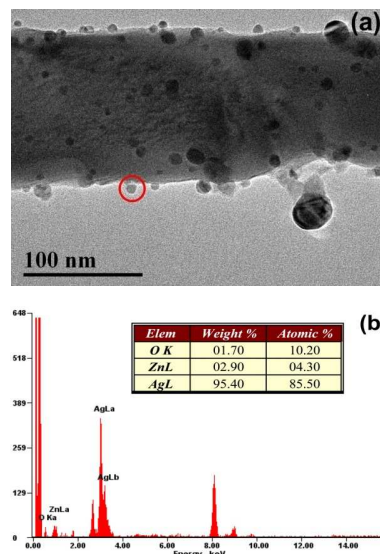


**Fig. 5** TEM image (a) and EDX spectra (b) of ZnO/Ag heterostructure sample 1.

In the Raman spectra (Fig. 6), the pure ZnO exhibits strong bands at  $583.1$ ,  $435.3$ ,  $382.0$ , and  $331.6$   $\text{cm}^{-1}$ , which are corresponding to the  $E_1$  (LO),  $E_2$ ,  $A_1$  (TO), and  $A_1$  modes of wurtzite ZnO respectively.<sup>17</sup> A stronger  $E_2$  mode and a much lower  $E_1$  mode indicate sample's good crystal quality with a low oxygen vacancy. As to ZnO/Ag heterostructure sample 1,  $E_2$  and  $A_1$  modes are significantly weaker than that of pure ZnO, and the  $A_1$  (TO) red shift by  $10$   $\text{cm}^{-1}$ . There is a new peak at  $480$   $\text{cm}^{-1}$  for sample 1 accompanying with the disappearance of  $E_1$  (LO) in the pure ZnO sample. The  $480$   $\text{cm}^{-1}$  peak enhancement in Raman spectra is most probably due to the local field enhancement induced by the surface plasmons of the metallic Ag on the surface of the ZnO/Ag heterostructures.<sup>4, 18</sup> As  $E_1$  (LO) mode is associated with oxygen deficiency,<sup>8</sup> the results reveal that the metallic Ag deposits around the sites of oxygen vacancy on the surface of ZnO, and then strong-bonded heterostructures form.

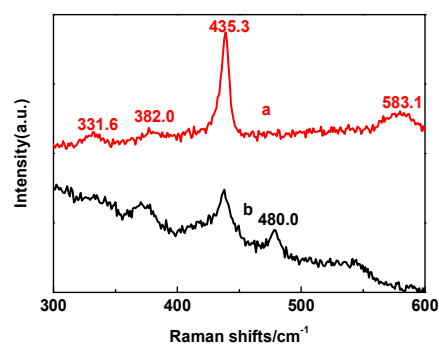


**Fig. 6** Raman spectra of pure ZnO (a) and ZnO/Ag heterostructure sample 1 (b).

The formation process of the close-bonded composition has also been studied by the control experiments, which were designed to investigate the influence of  $\text{Zn}(\text{NH}_3)_4^{2+}$  and temperature as described in experimental section. The XRD patterns of sample 2 and sample 3 are shown in Fig. 4B. Since sample 2 was washed before heated, hexagonal wurtzite ZnO was not detected

according to the XRD result, indicating the crucial role of  $\text{Zn}(\text{NH}_3)_4^{2+}$  for the formation of ZnO. In the case of lower temperature (100 °C), the product of sample 3 was composed of  $\text{Ag}/\text{Zn}_5(\text{OH})_8(\text{NO}_3)_2 \cdot 3\text{NH}_3 \cdot 7\text{H}_2\text{O}$  (JCPDF 40-1459). This result indicates that higher temperature is necessary for the removal of  $\text{NH}_3$  “bridge” and the preparation of ZnO. Then the formation process of the ZnO/Ag heterostructure was concluded as follows. First, the zinc powder dispersed in the Tollens' reagent replaces the  $\text{Ag}^+$ . The Ag nanoparticles are then produced and scatter in the solution of  $\text{Zn}(\text{NH}_3)_4^{2+}$ . By the thermal decomposition of  $\text{Zn}(\text{NH}_3)_4^{2+}$ , the ZnO nanorods grow up and link with the surrounding Ag nanoparticles. During this process,  $\text{NH}_3$  plays an important role for the formation of ZnO/Ag heterostructures due to its unique coordination to the surface of both ZnO and Ag. Accompanying the removal of  $\text{NH}_3$  “bridge” at high temperature, ZnO rods and Ag nanoparticles are close enough and strong bonds form.

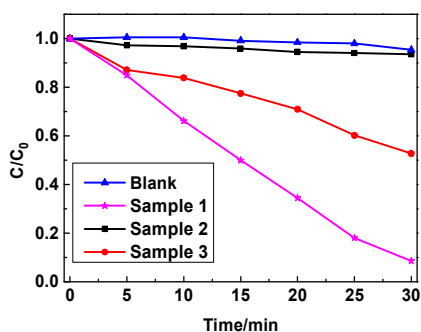


Fig.7 Photodegradation of XO over ZnO/Ag heterostructures sample 1, sample 2 and sample 3.

In addition, the catalytic performance of sample 2 and sample 3 were also investigated and the results are shown in Fig. 7. Compared with that of sample 1, the catalytic activity of sample 2 was negligible, and sample 3 revealed a moderate catalytic activity which was about half of the activity of sample 1. The photocatalytic performance could be explained by the UV-visible diffuse reflectance spectra of sample 2 and sample 3, which are shown in Fig. 2. There is a positive relationship between the absorbance in visible light range and the photocatalytic activity driven by visible light.

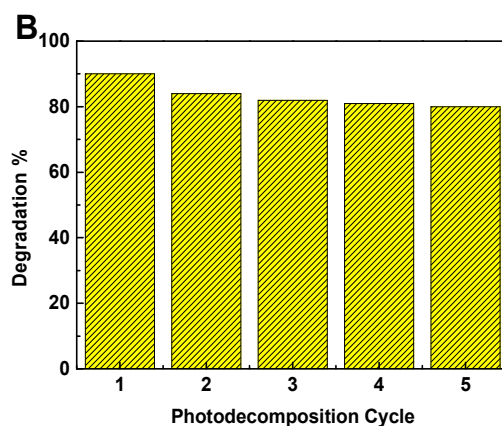
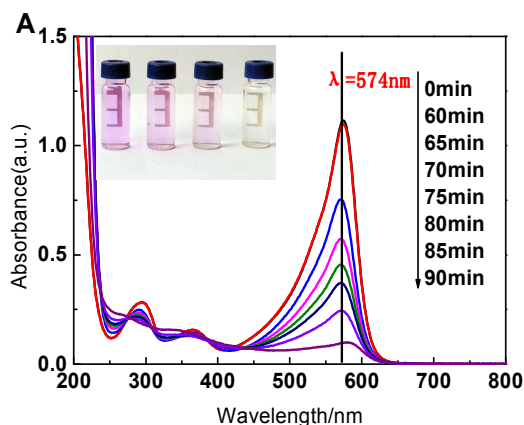


Fig. 8 A: Time-dependent UV-vis absorbance spectra of the XO solution in the presence of ZnO/Ag heterostructure sample 1. B: Photocatalytic behaviors of the ZnO/Ag heterostructure sample 1 for the degradation of XO in 5 consecutive cycles (the reaction time for each cycle was 30 min).

### 3.3 Photocatalytic application and mechanism

Photocatalytic activity of sample 1 under visible light (>420 nm) has been measured by degradation of XO dye as a model reaction (Fig. 3). From the time-dependent absorbance spectra in the presence of ZnO/Ag heterostructure (Fig. 8A), it can be seen that the absorbance peak at 574 nm decreased significantly and no new peak appeared between 250 nm and 800 nm, which indicated the degradation of the dye molecules. In addition, this catalyst can be used for multiple runs (Fig. 8B), and there is no obvious decrease in catalytic activity after five circles. Thus, this catalyst is very robust during photolysis, which could be due to its high crystallinity.

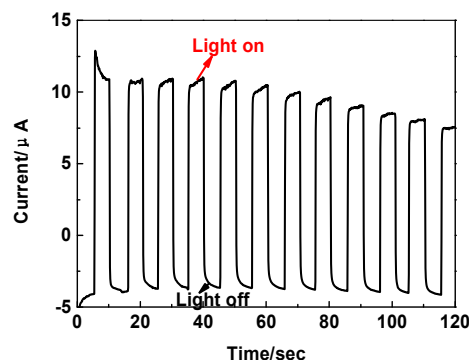
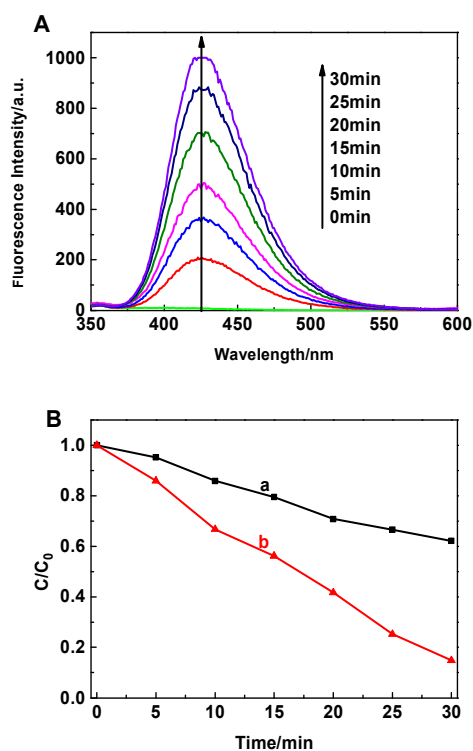


Fig. 9 Photoelectric conversion performances of ZnO/Ag heterostructure sample 1 in 0.1 mol/L  $\text{Na}_2\text{SO}_4$  aqueous solutions under visible light.

Owing to their intrinsic band-gap structure, semiconductors exhibit unique photoelectric property. This provides a simple and economical light-to-electric conversion approach for various energy-related applications.<sup>19</sup> To further investigate the photo-induced behaviors and photo-electrochemical property, the transient photocurrent responses of ZnO/Ag heterostructure sample 1 was measured via the on-off illumination under visible light. ZnO/Ag heterostructure sample 1 was deposited on indium tin oxide (ITO) glass before determination. As shown in Fig. 9, the ZnO/Ag heterostructures exhibit a remarkable photoelectric current. This is due to a good separation of the plasmon-induced

electron-hole pairs at the interface of Ag and ZnO. The electrons transfer from ZnO to ITO, while the holes moved to Ag surface are trapped by the electrolyte.

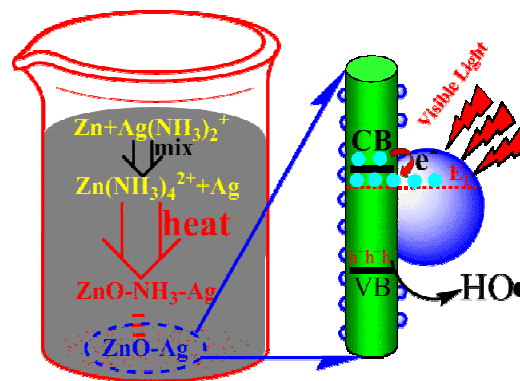
In the photocatalytic system for degradation of organic compound, there are two common routes: one is that organic molecule is oxidized by holes directly and the other is through the generation of oxidative radicals. Because the adsorption of XO on catalyst is negligible through the adsorption-desorption equilibrium in dark, XO dye could be oxidized by radicals in bulk solution. To determine the role of hydroxyl radical in photocatalytic degradation of dyes, terephthalic acid was used as a fluorescence probe.<sup>20</sup> The ZnO/Ag heterostructure sample 1 was illuminated in the terephthalic acid solution with the same light source. Gradual increase of the fluorescence intensity at 425 nm was observed with longer illumination time (Fig. 10A). This indicates the generation of  $\cdot\text{OH}$  during the illumination. Tert-Butanol as an effective hydroxyl radical scavenger is widely used to identify the existence of  $\cdot\text{OH}$  reactions.<sup>21</sup> In Fig. 10B, photodegradation of XO was largely inhibited by the addition of tert-Butanol. Hence the radical  $\cdot\text{OH}$  is one of the reactive species in the reaction. Thus, XO dye was degraded by the hydroxyl radicals diffused from the surface of catalyst to bulk solution.



**Fig. 10** A: Fluorescence spectra (excitation at 315 nm) during illumination of ZnO/Ag sample 1 in terephthalic acid ( $7.5 \times 10^{-4}$  mol/L); B: photocatalytic degradation curves of XO over ZnO/Ag catalyst under different conditions: with tert-Butanol (a), without tert-Butanol (b) under visible light ( $>420$  nm).

Due to the strong surface plasmon absorption of Ag nanoparticles, the ZnO/Ag heterostructure is visible light active. Because the bottom energy level of the conduction band (CB) of ZnO is higher than the new equilibrium Fermi energy level ( $E_f$ ) of ZnO/Ag heterostructure, the photoexcited electrons on the CB

can transfer from ZnO to the Ag nanoparticles, leading to the separation of electron-hole pairs and generation of  $\cdot\text{OH}$ .<sup>11,22</sup> As shown in Scheme 1, through the unique bridging effect of  $\text{NH}_3$ , ZnO rods and Ag nanoparticles are bonded closely. This incorporation results in the adjustment of band gap energy and influences the electron-transfer between ZnO and Ag,<sup>23</sup> which lead to high visible-light-driven catalytic activity and stability.



**Scheme 1** Proposed scheme for formation of ZnO/Ag heterostructure and mechanism of photocatalysis under visible light.

#### 4. Conclusions

A simple and one-pot synthesis method at mild conditions for visible light active ZnO/Ag heterostructure has been studied. By comparison of ZnO/Ag heterostructures with different Ag loading amounts, it was found that the XO visible-light photodegradation on the ZnO/Ag heterostructure was closely related to the Ag loading, and the sample with Zn/Ag of 4:4 revealed the best catalytic performance. The enhanced photocatalytic activity is mainly attributed to the band structure and intense localized surface plasmon resonance. Due to the strong surface plasmon absorption of Ag nanoparticles, the band gap of ZnO/Ag heterostructure with Zn/Ag of 4:4 is adjusted to 2.85 eV. Furthermore, the ZnO/Ag heterostructure shows a high separation efficiency of the photo-induced electron-hole pairs and generation of the hydroxyl radicals, which is important for the removal of organic pollutants by oxidation mechanism. Due to the bridging effect of  $\text{NH}_3$ , ZnO rods and Ag nanoparticles can link each other by strong bonds. The preparation method may open a new route for synthesis of metal/semiconductor heterostructures with desired properties.

#### Acknowledgement

The authors gratefully acknowledge the support from the National Natural Science Foundation of China (No. 20903048, 21005031, 21275065), the National Key Technology Research and Development Program (2012BAD32B03-4), the Fundamental Research Funds for the Central Universities (JUSRP51314B). The authors also thank Zhiji Han (University of Rochester, USA) for his kind help.

#### Notes and References

Key Laboratory of Food Colloids and Biotechnology (Ministry of Education of China), School of Chemical and Material Engineering Jiangnan University, Wuxi 214122, P. R. China.

Fax: (+) 86-510-85917763; E-mail: dongym@jiangnan.edu.cn

1. V. Subramanian, E. E. Wolf and P. V. Kamat, *J. Am. Chem. Soc.*, 2004, **126**, 4943-4950.
2. I. Jen-La Plante, S. E. Habas, B. D. Yuhas, D. J. Gargas and T. Mokari, *Chem. Mater.*, 2009, **21**, 3662-3667.
3. T. Arai, M. Horiguchi, M. Yanagida, T. Gunji, H. Sugihara and K. Sayama, *Chem. Commun.*, 2008, **43**, 5565-5567; W. Zhou, H. Liu, J. Wang, D. Liu, G. Du, S. Han, J. Lin and R. Wang, *Phys. Chem. Chem. Phys.*, 2010, **12**, 15119-15123; X. Yan, C. Zou, X. Gao and W. Gao, *J. Mater. Chem.*, 2012, **22**, 5629-5640.
4. Z. Mao, W. Song, L. Chen, W. Ji, X. Xue, W. Ruan, Z. Li, H. Mao, S. Ma and J. R. Lombardi, *J. Phys. Chem. C*, 2011, **115**, 18378-18383.
5. T. Mokari, C. G. Sztrum, A. Salant, E. Rabani and U. Banin, *Nat. Mater.*, 2005, **4**, 855-863; H. Zeng, W. Cai, P. Liu, X. Xu, H. Zhou, C. Klingshirn and H. Kalt, *ACS Nano*, 2008, **2**, 1661-1670; C. Gu, C. Cheng, H. Huang, T. Wong, N. Wang and T.-Y. Zhang, *Cryst. Growth Des.*, 2009, **9**, 3278-3285.
6. G. Merga, L. C. Cass, D. M. Chipman and D. Meisel, *J. Am. Chem. Soc.*, 2008, **130**, 7067-7076; Y. Zheng, L. Zheng, Y. Zhan, X. Lin, Q. Zheng and K. Wei, *Inorg. Chem.*, 2007, **46**, 6980-6986.
7. J. Das and D. Khushalani, *J. Phys. Chem. C*, 2010, **114**, 2544-2550.
8. R. Georgekutty, M. K. Seery and S. C. Pillai, *J. Phys. Chem. C*, 2008, **112**, 13563-13570.
9. P. V. Kamat, *J. Phys. Chem. B*, 2002, **106**, 7729-7744; J. A. Scholl, A. L. Koh and J. A. Dionne, *Nature*, 2012, **483**, 421-427.
10. P. Mulvaney, *Langmuir*, 1996, **12**, 788-800; C. J. Murphy, T. K. Sau, A. M. Gole, C. J. Orendorff, J. Gao, L. Gou, S. E. Hunyadi and T. Li, *J. Phys. Chem. B*, 2005, **109**, 13857-13870; Y. Nishijima, K. Ueno, Y. Yokota, K. Murakoshi and H. Misawa, *J. Phys. Chem. Lett.*, 2010, **1**, 2031-2036; P. Li, Z. Wei, T. Wu, Q. Peng and Y. Li, *J. Am. Chem. Soc.*, 2011, **133**, 5660-5663; Z. Yang, P. Zhang, Y. Ding, Y. Jiang, Z. Long and W. Dai, *Mater. Res. Bull.*, 2011, **46**, 1625-1631; R. Saravanan, S. Karthikeyan, V. Gupta, G. Sekaran, V. Narayanan and A. Stephen, *Mater. Sci. Eng., C*, 2013, **33**, 91-98;
11. M.-K. Lee, T. G. Kim, W. Kim and Y.-M. Sung, *J. Phys. Chem. C*, 2008, **112**, 10079-10082.
12. D. H. Yoo, T. V. Cuong, V. H. Luan, N. T. Khoa, E. J. Kim, S. H. Hur and S. H. Hahn, *J. Phys. Chem. C*, 2012, **116**, 7180-7184.
13. M. a. E. Aguirre, H. n. B. Rodriguez, E. San Román, A. Feldhoff and M. a. A. Grela, *J. Phys. Chem. C*, 2011, **115**, 24967-24974; C. Chen, Y. Zheng, Y. Zhan, X. Lin, Q. Zheng and K. Wei, *Dalton. Trans*, 2011, **40**, 9566-9570; Y. Yu, Y. Zuo, C. Li, J. Yang and C. Lu, *Nanoscale*, 2012, **4**, 5895-5901; H. Liu, G. Shao, J. Zhao, Z. Zhang, Y. Zhang, J. Liang, X. Liu, H. Jia and B. Xu, *J. Phys. Chem. C*, 2012, **116**, 16182-16190; F. Sun, F. Tan, W. Wang, X. Qiao and X. Qiu, *Mater. Res. Bull.*, 2012, **47**, 3357-3361.
14. Z. Han, L. Ren, Z. Cui, C. Chen, H. Pan and J. Chen, *Appl. Catal. B*, 2012, **126**, 298-305; A. A. Ashkarran, *Appl. Phys. A: Mater. Sci. Process*, 2012, **107**, 401-410; T.-J. Whang, M.-T. Hsieh and H.-H. Chen, *Appl. Surf. Sci.*, 2012, **258**, 2796-2801.
15. Y. Gao, W. Wu, D. Kong, L. Ran, Q. Chang and H. Ye, *Physica. E: Low. Dimens. Syst. Nanostruct.*, 2012, **45**, 162-165; M. Mahanti and D. Basak, *Chem. Phys. Lett.*, 2012, **542**, 110-116; J. Xin, K. Hui, K. Wang, H. L. W. Chan, D. H. C. Ong and C. Leung, *Appl. Phys. A: Mater. Sci. Process*, 2012, **107**, 101-107.
16. S. Zhang, C. Zhang, Y. Man and Y. Zhu, *J. Solid State Chem.*, 2006, **179**, 62-69.
17. L. Kong, Z. Jiang, T. Xiao, L. Lu, M.O. Jones, P.P. Edwards, *Chem. Commun.*, 2011, **47**, 5512-5514.
18. R. Wang, G. Xu and P. Jin, *Phys. Rev. B*, 2004, **69**, 113303.
19. A. Rumyantseva, S. Kostcheev, P.-M. Adam, S. V. Gaponenko, S. V. Vaschenko, O. S. Kulakovich, A. A. Ramanenka, D. V. Guzatov, D. Korbutyak and V. Dzhanan, *ACS nano*, 2013, **7**, 3420-3426.
20. S. Yang, J. Gong and Y. Deng, *J. Mater. Chem.*, 2012, **22**, 24522-24525; Q. Li, T. Gao, Y. Wang and T. Wang, *Appl. Phys. Lett.*, 2005, **86**, 123117-123113; L.-B. Luo, X.-B. Yang, F.-X. Liang, J.-S. Jie, Q. Li, Z.-F. Zhu, C.-Y. Wu, Y.-Q. Yu and L. Wang, *Cryst. Eng. Comm.*, 2012, **14**, 1942-1947.
21. J. Jiang, H. Li and L. Zhang, *Chem. Eur. J.*, 2012, **18**, 6360-6369.
22. A. L. Linsebigler, G. Lu and J. T. Yates Jr, *Chem. Rev.*, 1995, **95**, 735-758; X. Li and F. Li, *Environ. Sci. Technol.*, 2001, **35**, 2381-2387.
23. J. Chiou, S. Ray, H. Tsai, C. Pao, F. Chien, W. Pong, C. Tseng, J. Wu, M. H. Tsai and C. H. Chen, *J. Phys. Chem. C*, 2011, **115**, 2650-2655.

A simple, mild and large-scale one-pot synthesis method for visible light active ZnO/Ag heterostructures was proposed

